Interface-engineered 3D-printed PCEC/Collagen composite scaffold for large bone defect repair under static and mechanical stimulation

Yu-Yao Liu[1,2], Marko Dobricic[3,4,5], Claudio Intini[3,4,5,6], Fergal J. O'Brien[3,4,5 *], Javier LLorca[1,2*] and Mónica Echeverry-Rendón[1*]

[1] IMDEA Materials Institute, 28906 Getafe, Madrid, Spain

[2] Department of Materials Science, Polytechnic University of Madrid/Universidad Politécnica de Madrid, 28040 Madrid, Spain

[3] Tissue Engineering Research Group, Department of Anatomy & Regenerative Medicine, Royal College of Surgeons in Ireland (RCSI), Dublin, Ireland

[4] Trinity Centre for Biomedical Engineering, Trinity College Dublin (TCD), Dublin 2, Ireland

[5] Advanced Materials and Bioengineering Research (AMBER) Centre, RCSI and TCD, Dublin, Ireland

[6] Department of Biomedical Sciences, University of Cagliari, Cittadella Universitaria, 09042 Monserrato, Italy

Abstract

The repair of large traumatic bone defects remains a huge challenge in orthopedic clinics due to the complicated environment of bone healing involving bone regeneration and vascularization in the defect region. This is even more pronounced with an aging population worldwide. To address this, a novel interface-engineered scaffold was developed by integrating a bone-mimetic collagen type I/nano-hydroxyapatite (CI-nHA) matrix with a 3D-printed poly(ε-caprolactone)-polyethylene glycol 20k-poly(ε-caprolactone) (PCL-PEG20k-PCL, $PCE_{20k}C$) triblock copolymer framework. The scaffold formed biofunctional interfaces with both enhanced mechanical support and promoted cell-material interaction. It exhibited interconnected multi-scale pores and a compressive modulus of ~37 MPa, comparable to cancellous bone. After culturing with preosteoblast (MC3T3) under osteogenic conditions for 4 weeks, it showed promoted osteoblast proliferation, differentiation and matrix mineralization. The reinforced architecture further upregulated osteogenic transcription factors of RUNX2 and BMP-2. Moreover, when cultured with endothelial cells, it promoted early angiogenic activity within 5 days, indicating interface-mediated vascularization. Furthermore, when subjected to mechanical stimulation in a bioreactor with simulated physiological mechanical condition, the reinforced scaffold supported osteoblast viability and enhanced early mineralization evidenced by increasing gene expression of ALP and OCN after 1 week of intermittent mechanical stimulation. Overall, this interface-engineered scaffold integrates precise 3D architecture with collagen-functionalized surfaces to effectively support bone regeneration and angiogenesis under both static and mechanical conditions,

highlighting its translational potential for large bone defect repair.

Keywords: $PCE_{20k}C$ copolymer; Collagen type I and nano-hydroxyapatite matrix; Biofunctional interfaces; Osteogenesis; Angiogenesis; Mechanical stimulation

1. Introduction

Large bone defects caused by trauma, disease, injury or infection are particularly challenging to heal, especially when they exceed the critical self-regeneration threshold (> 2.5 cm). In such cases, the implantation of substitutes becomes necessary, posing a significant clinical challenge [1][2]. Autografts and allografts are considered the most effective methods for treating bone defects. However, their clinical application is severely limited by several drawbacks such as resource scarcity, immune rejection, and infection risks [3]. To address these challenges, tissue-engineered scaffolds composed of metals, ceramics, and polymers have emerged as promising alternatives [4][5]. Despite notable progress, many implants still fail to match the mechanical properties, biological functionality and degradation rates of native bone tissue, significantly limiting their effectiveness [6]. For instance, titanium and its alloys are widely used in clinical settings due to their high mechanical strength. However, their non-degradable nature leads to a second surgery for implant removal after bone healing, which is associated with severe pain and infection risks. Additionally, stress concentration can result in implants loosening and fracture [7][8]. Therefore, there is an urgent need to develop biodegradable scaffolds with appropriate mechanical properties, biological functionality and degradation rates comparable to those of native tissue.

3D printing technology enables the precise and rapid fabrication of scaffolds that closely mimic native bone tissues at macro and micro architectures. In particular, it can achieve interconnected pore design, which is conducive to cell growth and vascularization during bone regeneration [9][10]. Biodegradable synthetic polymers have been extensively explored in bone tissue engineering due to controlled composition, flexible processing, and no immunological concern [11][12]. Among them, polycaprolactone (PCL) has attracted substantial interest due to its biocompatibility, mild processing condition (melting point: 50 - 60 °C), and non-inflammatory degradation products [13][14]. However, its hydrophobic nature results in a slow degradation rate of 2-3 years *in vivo*, severely limiting its clinical applications [15]. To overcome this limitation, our previous work synthesized a series of poly(ε-caprolactone)-poly(ethylene glycol)-poly(ε-

caprolactone) (PCEC) copolymers using hydrophilic PEG with macroinitiators [16]. Among them, $PCE_{20k}C$ shows excellent potential for bone tissue engineering. Its pronounced shear-thinning behavior enhances its processability in extrusion-based 3D printing. More importantly, it exhibits a significantly lower water contact angle of (45.2°) compared with PCL (84.2°), leading to a faster degradation rate of 60% mass loss after 8 hours, compared to 70% mass loss after 23 days for PCL under accelerated degradation conditions. However, similar to PCL, $PCE_{20k}C$ lacks bioactive sites, which limit osteogenesis, osteointegration, and osteoconductivity.

Recent research has shifted towards biomimetic composite scaffolds, which integrate bioactive matrices with native tissue-derived compounds into 3D printed frameworks. This approach maintains mechanical properties while improving overall performance in aspects such as chondrogenesis and osteogenesis [17][18]. Hydroxyapatite (HA) and collagen type I (CI), the primary components of bone tissue, have been widely incorporated into bone tissue-engineered scaffolds. Their combination has demonstrated significant efficacy in promoting bone regeneration [19][20]. For example, Cunniffe et al. [21] have shown that addition of nano HA (nHA) particles to highly porous collagen scaffolds significantly accelerate *in vivo* bone formation and healing in a critical-sized rat calvarial defect. Moreover, CI-nHA scaffolds have been frequently used as a bone layer matrix, and they have been demonstrated excellent *in vitro* and *in vivo* performance in a variety of animal models, including rabbits and horses[22][23] . Despite these advances, the mechanical properties of CI-nHA scaffolds remain inferior to those of native bone, limiting their application to small defect repair. Therefore, this study aims to incorporate 3D-printed $PCE_{20k}C$ framework to reinforce CI-nHA matrix, ultimately combining sufficient mechanical support and specific bioactivity targeting the large bone defect repair.

Beyond scaffold composition, external mechanical stimulation also plays a crucial role in bone defect repair. Native bone tissue continuously experiences mechanical stress from physical activities such as bending, compression, and shear forces [24]. Wolff et al. [25] demonstrated that bone is a dynamic organ capable of responding to mechanical and biophysical stimuli. Through mechanotransduction, bone cells convert mechanical signals into molecular and biological responses, initiating bone regeneration by activating osteoblasts for matrix deposition [26]. However, most *in vitro* cell culture studies are conducted under static conditions, failing to replicate the motive mechanical environment of living tissues. Bioreactors have been developed

to simulate physiological conditions while preserving 3D characteristics that are difficult to replicate in traditional cell cultures. Diverse stimulation strategies such as electrical, perfusion, or compression/stretching have been utilized in bioreactors for better mimicking the physiological environment [26] [27] [28]. For example, Teoh et al. [29] investigated the effect of *in vitro* cyclic compression on the osteogenesis of 3D-printed poly(caprolactone)-β-tricalcium phosphate (PCL-TCP) scaffolds seeded with mesenchymal stem cell (MSC). Their results showed that dynamic loading increased alkaline phosphatase (ALP) activity by 3.76-fold and calcium deposition by 1.96-fold compared to static culture within 14 days, highlighting the importance of mechanical stimulation in early osteogenesis. Therefore, it is important to consider the effect of dynamic mechanical stimulation *in vitro* on the osteogenesis of cell-laden scaffolds, which also lays the foundation for evaluating the potential of scaffolds under physiological motive environments.

Herein, this study aims to fabricate a composite scaffold consisting of a 3D-printed porous $PCE_{20k}C$ framework and a bioactive CI-nHA matrix specifically designed for bone defect repair. The compressive properties of the scaffold were evaluated both in dry and wet conditions. Degradation behavior was systematically in phosphate-buffered saline (PBS) solution at 37 °C over eight weeks, examining changes in structure, mass, pH and mechanical properties. Additionally, *in vitro* studies assessed osteogenic and angiogenic potential using pre-osteoblast MC3T3 and endothelial EA.hy 926 cells. Finally, a seven-day dynamic compression culture in a bioreactor was conducted to investigate the effects of mechanical stimulation on the cell viability and osteogenesis of cell-seeded composite scaffolds.

2. Materials and Methods

2.1 Fabrication of collagen-incorporated $PCE_{20k}C$ composite scaffold

2.1.1 Synthesis of $PCE_{20k}C$ copolymer

$PCE_{20k}C$ (Mw= ~ 80,000 g/mol) was synthesized through the ring-opening reaction of PEG and ε-CL, according to our previous research [16], as shown in Scheme 1. Specifically, 20 g of Ɛ-caprolactone (Ɛ-CL, 97%, distilled before use, Sigma-Aldrich, Germany), and 4 g of PEG20k (Mn=20,000 g/mol, dried before use, Sigma-Aldrich, Germany) were mixed with a 0.5 wt% of the catalyst of tin (II) 2-ethylhexanoate ($Sn(Oct)_2$, 92.5-100%, Sigma-Aldrich, Germany) in a Schlenk flask. The flask was then well-sealed and heated to 110 °C for 24 h after removing moisture and oxygen using a vacuum pump. After the reaction, the product was dissolved in dichloromethane

(CH_2Cl_2, 99.0%, anhydrous, TCI EUROPA N.V., Belgium) and then precipitated in petroleum ether (boiling point ≥90% 40-60 °C, Sigma-Aldrich, Germany). This process was repeated three times to remove the catalyst. Finally, the product was dissolved again in CH_2Cl_2 and poured into flat plates to obtain $PCE_{20k}C$ thin films, which were dried overnight in a fume hood. The dried $PCE_{20k}C$ thin films were then cut into small pieces to form pellets for 3D printing.

2.1.2 Manufacture of 3D printed $PCE_{20k}C$ scaffold

The pellets of $PCE_{20k}C$ copolymer were poured into a screw-assisted extrusion-based 3D printer (F40, Direct 3D, Italy) equipped with a 500 μm nozzle to manufacture porous $PCE_{20k}C$ scaffolds. The extruder of the printer was set to a printing temperature of 90 °C, a movement speed of 10 mm/s, and a flow rate of 2,000 %. After preheating for 30 min, the molten material was deposited layer by layer in a 0°/90° laying pattern to fabricate a scaffold with a filament diameter of 500 μm, a filament spacing of 1,000 μm and a final height of 3 mm. Finally, the scaffold was cut using a biopsy puncher (Kai Medical, Japan) with a 6 mm diameter to obtain the cylindrical structure.

2.1.3 Preparation of the collagen-based composite scaffold

A collagen-based slurry consisting of collagen type I and nano-hydroxyapatite (CI-nHA) was prepared according to previously established methods [21]. Briefly, a calcium chloride solution ($CaCl_2$, 0.13M, Fisher Chemical, Ireland) was added to a trisodium phosphate solution (Na_3PO_4, 0.42M, Sigma-Aldrich, Ireland) with sodium hydroxide (NaOH, Fisher Chemical, Ireland) and DARVAN® 821-A (R.T. Vanderbilt Holding Company, Inc, USA) at a ratio of 1.67 between Ca/P atoms molarity, then followed by stirring overnight. The mixture was then centrifuged to remove the supernatant and resuspended in water, repeating this process three times. Then n-HA suspension was obtained by resuspending the precipitate in acetic acid (0.5M, Sigma-Aldrich, Ireland) and sonicating for 2-3 minutes. Finally, the n-HA suspension was added dropwise to 300 mL of collagen type I (lyophilized polymeric collagen, Sigma-Aldrich, Ireland) in acetic acid slurry, followed by blending for 2 h to obtain a homogenous CI-nHA slurry.

The 3D-printed $PCE_{20k}C$ scaffolds were placed in a stainless-steel plate with holes of 9.5 mm in diameter and 4 mm in height, and 300 μL of the prepared CI-nHA slurry was added to cover the scaffold. The plate was then placed in a freeze-dryer (Virtis Genesis 25EL, Biopharma, UK) and processed under controlled conditions, a constant cooling rate of 1 °C/min, a final temperature of

- 40 °C and a pressure of 200 mTorr for 40 h. The final composite scaffolds measuring 6 mm in diameter and 3 mm in height, were obtained using a 6 mm biopsy puncher. For comparation, CI-nHA scaffolds without 3D printed frameworks were also fabricated through the same methods and subjected to an additional treatment of a dehydrothermal (DHT) cross-linking procedure in a vacuum oven at 105 °C under 0.05 bar pressure for 24 h.

2.2 Material Characterization

2.2.1 Composition and structure

The morphology of CI-nHA, $PCE_{20k}C$, and composite scaffolds in both top and cross-sectional views was observed using a field emission scanning electron microscope (FESEM, JSM-7800 F, ThermoFisher) with an acceleration voltage of 5.0 kV and a current of 0.1 nA. The calcium distribution in CI-nHA, $PCE_{20k}C$, and composite scaffolds were analyzed using energy-dispersive X-ray spectroscopy (EDS) in the FESEM with an EDS detector.

2.2.2 Mechanical characterization

All scaffolds with cylindrical shapes of a diameter of 6 mm and a height of 3 mm were tested under dry (air) and wet conditions (PBS solution). The mechanical properties of both original and degraded CI-nHA scaffolds were evaluated in a bioreactor (TC-3F, Ebers, Spain) using a 50 N load cell and compressive grips. The mechanical properties of both original and degraded $PCE_{20k}C$ and composite scaffolds were tested using a universal testing system (Instron 5966, USA) with a 2 kN load cell and compressive grips. Scaffolds for wet condition tests were immersed in 0.1M phosphate-buffered saline (PBS, Gibco, UK) solution overnight before testing. Each sample was tested using at least six scaffolds to obtain an average value.

2.3 *In vitro* degradation test

The *in vitro* degradation properties were assessed by immersing CI-nHA, $PCE_{20k}C$, and composite scaffold in 0.1 M PBS solution (pH = 7.20) at 37 °C for eight weeks, following the international standard ISO 13781 [30]. The PBS volume-to-scaffold mass ratio was maintained at a minimum of 30 mL/g. Scaffolds were removed at weeks 1, 2, 4, 6 and 8, washed with deionized water, and

dried in a fume cabinet overnight. Mass change and pH variation were recorded at each time point. Each sample was tested using at least three scaffolds per timepoint to obtain an average value.

2.4 Osteogenic differentiation study

2.4.1 Cell culture

The mouse preosteoblast cell line MC3T3-E1 (ATCC-2593, USA) was expanded in completed culture medium (Minimum Essential Medium Eagle Alpha (α-MEM, Biosera, France) supplemented with 10 % fetal bovine serum (FBS), and 100 U/mL penicillin/streptomycin (P/S)) until reaching 80-90% confluence. Then, MC3T3 cells were seeded onto scaffolds at a density of 5×10^5 cells per scaffold placed into a 24-well plate and cultured in 2 mL of completed culture medium under conditions of 37 °C and 5 % CO_2. The cell-seeded scaffold was transferred to a new plate after one day of seeding and 2 mL of osteogenic culture medium (α-MEM supplemented with 10% FBS, 100 U/mL P/S, 50 μg/mL L-ascorbic acid, 10 mM β-glycerophosphate, and 100 nM dexamethasone, additives are all from Sigma-Aldrich, Ireland) was added. Incubation continued for 28 days, with the osteogenic culture medium changed every 3 to 4 days.

2.4.2 Evaluation of metabolic activity

The metabolic activity of scaffolds was measured by AlamarBlue assay. On days 1, 3, 7, 14, 21, and 28, scaffolds were washed with PBS and placed in 1 mL of osteogenic medium containing 10% Alamar Blue reagent (ThermoFisher Scientific, Ireland) at 37 °C for 3 h. Then, fluorescence levels of the extracts were measured using a microplate reader (Tecan Infinite M Plex, Switzerland) at an excitation wavelength of 550 nm and an emission wavelength of 590 nm. Extracts without scaffolds were used as blank, and the extracts of CI-nHA scaffold at day 1 served as the control. Metabolic activity was calculated after normalizing the optical density (OD) with respect to the control using the formula: metabolic activity (%) = (OD of sample - OD of blank) / OD of control × 100 %.

2.4.3 DNA quantification

The Quant-iT™ PicoGreen™ dsDNA Assay Kits and dsDNA Reagents (Invitrogen, USA) were used to quantify the DNA content of cells on scaffolds. On day 28, scaffolds were washed with

PBS and placed in 1 mL of lysis buffer consisting of 1% Triton X-100 (Sigma-Aldrich, Ireland) and 0.2 M sodium carbonate (Fisher Scientific, Ireland). After three freeze-thaw cycles at room temperature and - 80 °C, the solutions obtained were used for DNA quantification. The solutions from the ALP lysis buffer were used to measure DNA content on days 7 and 14.

2.4.4 Evaluation of alkaline phosphatase (ALP) activity

The SensoLyte pNPP Alkaline Phosphatase Assay Kit Colorimetric (AnaSpec, USA) was used to assess the ALP activity. On days 7 and 14, scaffolds were washed with PBS and placed in 200 µL lysis buffer containing 2% Triton X-100 and 0.1 M sodium acetate (Sigma-Aldrich, Ireland). Following by centrifugation at 10,000 g at 4 °C for 10 min, the obtained solutions were used to detect ALP activity using the assay kit.

2.4.5 Evaluation of mineralization

The Calcium (CPC) LiquiColor® Test Kit (Stanbio, USA) was used to quantify the calcium content in scaffolds to assess the mineralization. On days 21 and 28, both cell-free and cell-seeded scaffolds were washed with PBS and placed in 1 mL of 0.5 M HCl solution (Honeywell Fluka, ThermoFisher Scientific, UK). After overnight shaking at 4 °C, the obtained solutions were diluted 10-fold before calcium content detection using the assay kit.

2.4.6 Histological analysis

Histological staining was conducted to evaluate cellular infiltration and calcium distribution within scaffolds. Briefly, cell-seeded scaffolds were first fixed in formalin (Epredia™, ThermoFisher Scientific, Ireland) for 1 h, then immersed in 15% sucrose solution (Sigma-Aldrich, Ireland) for 4 h, followed by immersion in 30% sucrose solution overnight. The samples were then embedded in OCT (Fisher-Scientific, Ireland), and 10 µm thick slices were mounted on Polysine™ glass slides using a cryostat (Leica RM 2255, Leica, Germany).

Slices were stained with hematoxylin & eosin (H&E, Sigma-Aldrich, Ireland) to visualize cell infiltration (nuclei-stained dark purple), while with alizarin red S (Sigma-Aldrich, Ireland) to detect calcium deposits (stained red), respectively. Histological staining images were obtained under an inverted microscope (Leica Microsystems, Switzerland).

2.4.7 Quantitative real-time PCR (qRT-PCR) analysis

Gene expression levels of specific markers associated with osteogenic lineage were analyzed in scaffolds after 21 days in culture. Total RNA was previously isolated and reverse-transcribed into cDNA at a final concentration of 2.5 ng/µL using the QuantiTect Reverse Transcription kit (Qiagen, UK). The cDNA was then analyzed using the 7500 Real-Time PCR System (Applied Biosystems, USA). The relative expression of mRNA was assessed using the delta-delta Ct (ΔΔCt) method. Four genes associated with osteogenesis (COL1A1, RUNX 2, OCN and BMP-2, primers were all from QuantiTect Primer Assays, UK) detected using GAPDH as the housekeeping gene, as shown in Table S1.

2.5 Angiogenic differentiation study

Human endothelial cell line EA.hy 926 (ATCC-CRL-2922, USA) was used to assess angiogenesis. Briefly, EA.hy 926 cells were seeded at a density of 1×10^5 cells per scaffold in a 24-well plate and cultured in 2 mL of growth medium (high-glucose Dulbecco's Modified Eagle's Medium (DMEM, Biowest, France), supplemented with 10 % FBS, and 100 U/mL P/S) under conditions of 37 °C and 5 % CO_2. After 24 h, scaffolds were transferred to new plates and cultured for 5 days, with media change every 2 to 3 days. After 1 and 5 days of incubation, cells were stained with Alexa Fluor 488 phalloidin (1:300, Invitrogen, USA) and DAPI (1:1000, Invitrogen, USA) and then observed under a confocal microscope (Olympus FV3000, Japan) at magnification of 10x and 20x. Finally, three angiogenesis-related genes (VEGF, VE-cadherin (Integrated DNA Technologies, Belgium), and MMP-2 (Sigma, USA)) were evaluated by qRT-PCR, as shown in Table S2.

2.6 Mechanical stimulation in a bioreactor

A bioreactor (TC-3F, Ebers, Spain) with dynamic compression system was used to apply mechanical stimulation in an incubator under conditions of 37 °C and 5 % CO_2. Composite scaffolds were seeded with MC3T3 cells at a density of 5×10^5 cells per scaffold. After 7 days of pre-culture in a 24-well plate, cell-seeded scaffolds were transferred to bioreactor chambers filled with 25 mL of culture medium. After an overnight incubation, dynamic compression was applied with a displacement of 0.1 mm at a frequency of 1 Hz for 2 h per day for 7 days. The culture

medium was changed every 3-4 days. Metabolic activity of scaffolds was measured by AlamarBlue assay after seeding, before mechanical stimulation and after mechanical stimulation. Gene expression was tested after 7 days of mechanical stimulation. For comparison, different conditions in chambers were defined, as shown in Figure 7a, where chamber A was filled with complete medium and subjected to compression (named mechanical stimulation**)**, chamber B was filled with osteogenic medium without compression (named chemical stimulation), and chamber C was filled with osteogenic medium and subjected to compression (named double stimulation).

2.7 Statistical analysis

All data were presented as mean ± standard deviation unless stated otherwise. Origin software (2021b, OriginLab, USA) and GraphPad Prism (GraphPad Software 10.2.0, USA) were used for data analysis. A t-test was performed for two comparisons, and a one-way ANOVA analysis for multiple comparisons. $p \leq 0.05$ were considered statistically significant. Notes, ns $p > 0.05$, * $p \leq 0.05$, ** $p \leq 0.01$, *** $p \leq 0.001$ and **** $p \leq 0.0001$.

3. Results

3.1 Fabrication and Morphology

To create the composite scaffold, a 3D-printed $PCE_{20k}C$ framework was first manufactured as the mechanical support, which was designed from a copolymer synthesized using PEG and ε-CL. Then, a bioactive slurry (CI-nHA) composed of collagen type I and nano-hydroxyapatite, was prepared as biological cues. Finally, the biomimetic composite scaffold was obtained by soaking the $PCE_{20k}C$ scaffold in CI-nHA slurry after a further freeze-drying process, as shown in Scheme 1.

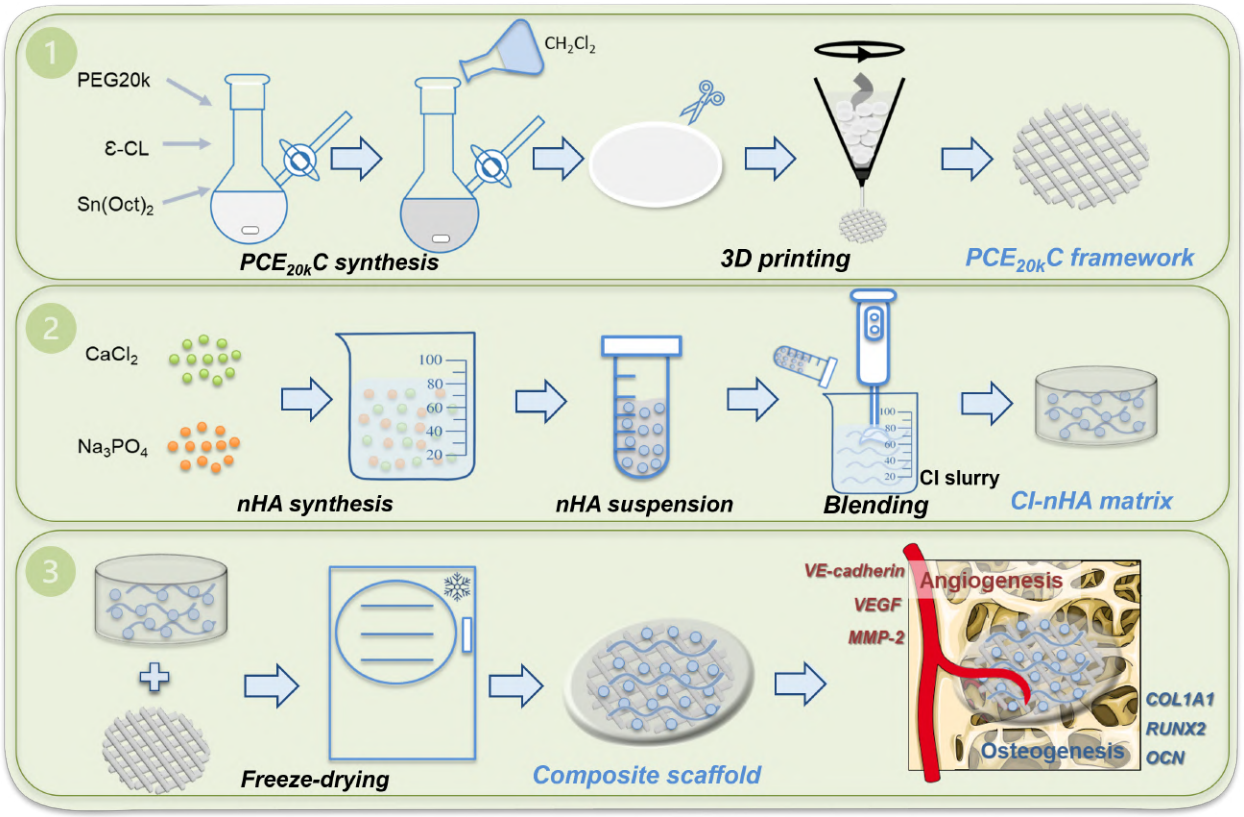

Scheme 1. Fabrication of the composite scaffold from $PCE_{20k}C$ framework and CI-nHA matrix.

The morphology of CI-nHA, $PCE_{20k}C$, and composite scaffolds were first studied from both top and section views (Figure 1). The collagen matrix exhibited a uniform porous structure with a mean micropore size of approximately 100 μm [31]. In the 3D-printed $PCE_{20k}C$ framework, the printed filaments had smooth, regularly shaped cylindrical structures with a diameter of 550 μm. The size of the interconnected macropores created by 3D printing was about 963 μm. After incorporation of collagen, the $PCE_{20k}C$ filaments were surrounded by the CI-nHA matrix without any clamping or deformation. Additionally, the CI-nHA matrix filled the 3D-printed macropores while preserving its original microporous structure. The calcium distribution in these scaffolds was characterized by EDS (Figure S1). The EDS map of the composite scaffold clearly shows a distinct dividing line, where calcium is evenly dispersed in the CI-nHA matrix, with almost no signal detected in the $PCE_{20k}C$ framework. These results confirm the successful fabrication of a biomimetic composite scaffold with hierarchical porosity and uniform calcium distribution.

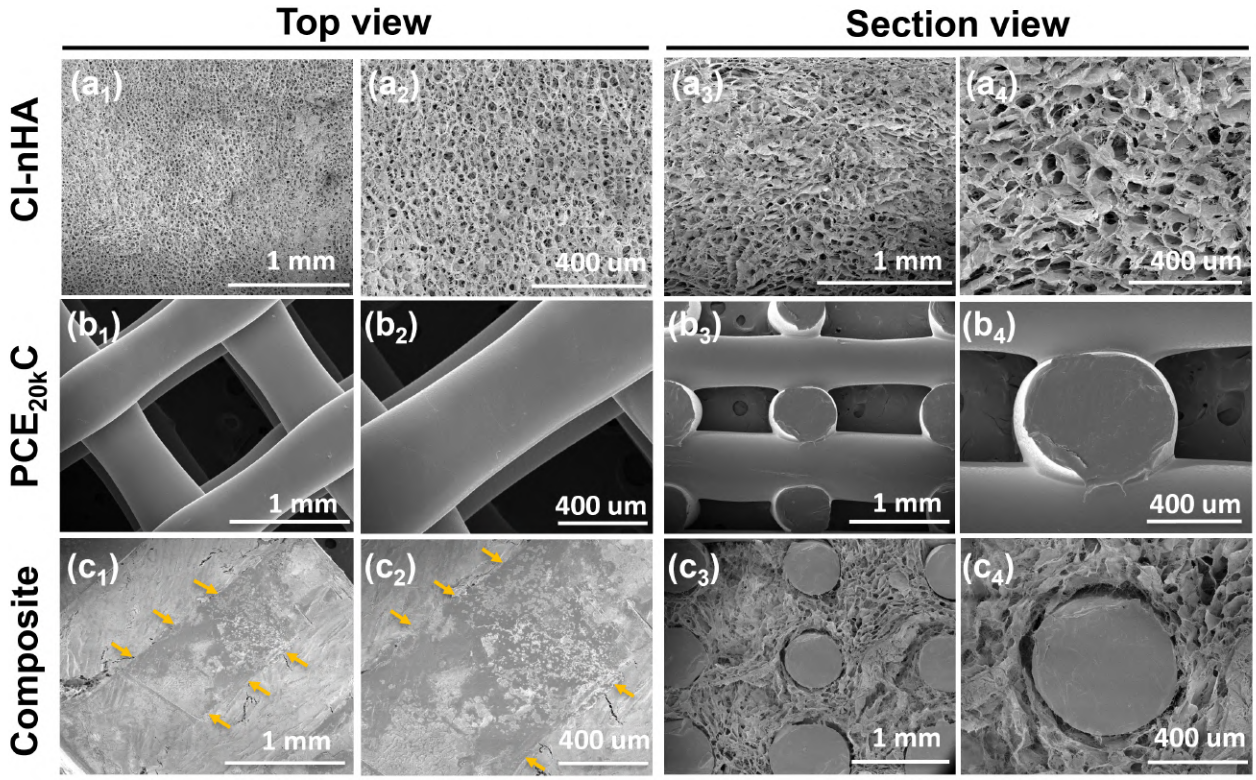

Figure 1. Scanning electronic microscopy (SEM) images of (a) CI-nHA matrix, (b) $PCE_{20k}C$ framework, and (c) the composite scaffold in both top view and section view.

3.2 Mechanical properties under both dry and wet conditions

Figure 2a shows the compression modulus of CI-nHA, $PCE_{20k}C$, and composite scaffolds in air (dry) and in PBS solution (wet). The CI-nHA scaffold exhibited a modulus of 26 kPa, significantly lower ($p < 0.0001$) than $PCE_{20k}C$ scaffold, which was 36.9 MPa in the dry condition. Notably, the incorporation of the CI-nHA matrix did not affect the mechanical properties of the composite scaffold, which maintained a modulus of 37.0 MPa, comparable to that of $PCE_{20k}C$ framework. Moreover, while the modulus of CI-nHA slightly decreased under wet conditions, the compression modulus of both the $PCE_{20k}C$ and composite scaffolds was similar to those found under dry conditions, as summarized in Table 1. These results confirm that the mechanical reinforcement of the composite scaffold originates from the $PCE_{20k}C$ framework.

Table 1 Compressive parameters of CI-nHA, $PCE_{20k}C$, and composite scaffolds in dry and wet conditions

Sample	Compressive modulus (MPa)	Compressive stress (MPa)
CI-nHA	0.026 ± 0.004	0.020 ± 0.002
CI-nHA wet	0.017 ± 0.006	0.005 ± 0.001
$PCE_{20k}C$	36.9 ± 0.8	5.24 ± 0.28
$PCE_{20k}C$ wet	37.1 ± 2.1	7.04 ± 0.17
Composite	37.0 ± 5.5	7.75 ± 1.20
Composite wet	35.1 ± 8.1	6.49 ± 0.70

3.3 *In vitro* degradation tests in PBS solution at 37ºC

The degradation of CI-nHA, $PCE_{20k}C$, and composite scaffolds was studied by immersion in PBS solution at 37 °C for 8 weeks. Throughout this period, all scaffolds maintained their macrostructural stability, as shown in Figure S2. The mass of all scaffolds gradually decreased over time, with final residue percentages of 60.7% for CI-nHA, 88.5% for $PCE_{20k}C$, and 92.1% for composite scaffolds after 8 weeks (Figure 2b). Notably, the pH of the $PCE_{20k}C$ scaffold dropped rapidly from 7.15 to 3.97 within the first week and continued declining to 3.28 by week 8, creating an acidic environment. In contrast, the incorporation of the CI-nHA matrix helped mitigate this acidity, resulting in the highest mass retention and a more stable, mild pH profile in the composite scaffold (Figure 2c).

Further degradation analysis was conducted by monitoring changes in compressive modulus and stress over time. The modulus and stress of the collagen matrix gradually decreased during degradation, whereas the $PCE_{20k}C$ framework retained its mechanical stability with no significant changes (Figure 2d and e). Interestingly, while the modulus of composite scaffold was maintained throughout the degradation period (Figure 2f), its structural integrity weakened, as indicated by the stress-stain curve (Figure S3), where the scaffold fractured in compression beyond 20% of strain at week 8. These findings demonstrate that although the composite scaffold maintained structural, mass, pH, and mechanical stability, significant degradation occurred after 8 weeks.

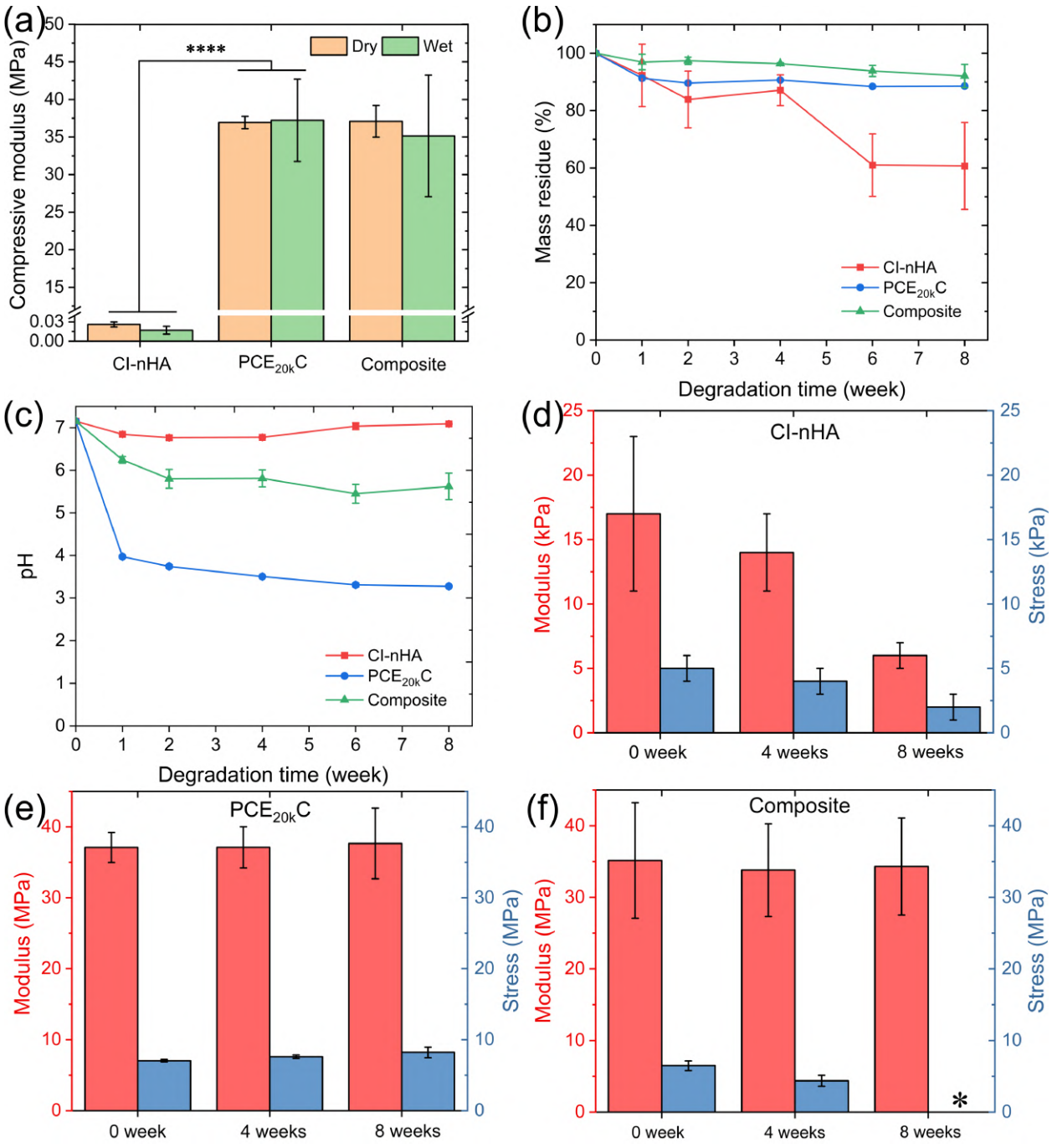

Figure 2. (a) Compressive modulus in dry and wet conditions, (b) pH change, and (c) mass retention of CI-nHA, $PCE_{20k}C$, and composite scaffolds. Compressive modulus and stress variations of (d) CI-nHA, (e) $PCE_{20k}C$, and (f) composite scaffolds after degradation at 0, 4, and 8 weeks.

3.4 Osteoblast cell viability and infiltration

To assess biocompatibility, the effect of the $PCE_{20k}C$ framework on cell viability and infiltration was evaluated by seeding MC3T3 pre-osteoblast cells onto CI-nHA and composite scaffolds. The $PCE_{20k}C$ framework alone was not included in the study, as its 3D-printed surface is too smooth to effectively support cell adhesion and growth. Results of metabolic activity over time show that $PCE_{20k}C$ framework did not affect MC3T3 cell viability, evidenced by no negative trend (Figure 3a). This was further confirmed by no significant difference observed between the CI-nHA and composite groups in metabolic activity and DNA content (Figure 3b). The composite scaffold exhibited a DNA content of 160.2 ng/mL on day 28, which is comparable to that of CI-nHA scaffold (166.1 ng/mL), indicating that the $PCE_{20k}C$ framework does not compromise the biocompatibility.

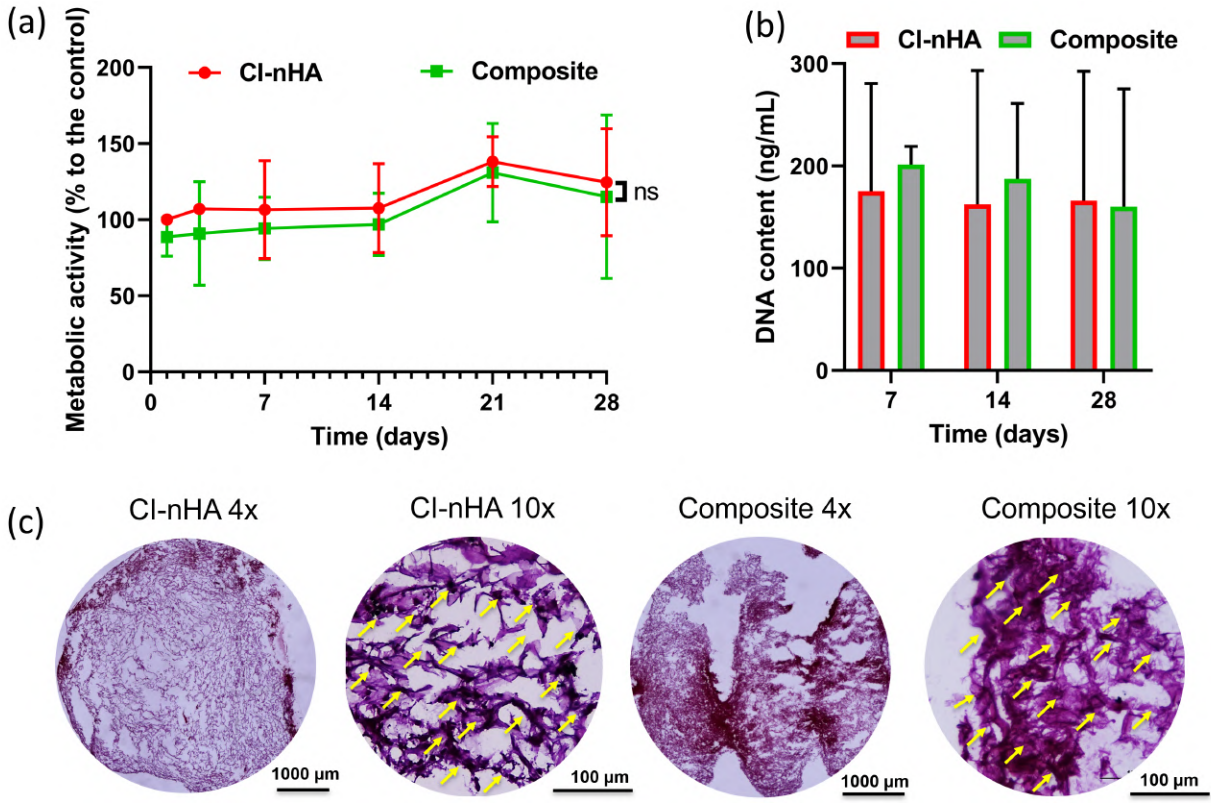

Figure 3. (a) Cellular metabolic activity (normalized to CI-nHA scaffolds at day 1) measured over 1, 3, 7, 14, 21, and 28 days, (b) DNA content per scaffold after 7, 14, and 28 days of culture and (c) H&E histological staining of both scaffolds after 28 days in culture.

Additionally, H&E staining revealed cell infiltration within the scaffolds. As shown in Figure 3c, cells were primarily localized at edges and gradually migrated inward in CI-nHA scaffold. In contrast, cell infiltration was observed in the composite scaffold not only along the scaffold edges but also in areas in direct contact with $PCE_{20k}C$ filaments. These findings demonstrate that the composite scaffold effectively support MC3T3 cell viability and infiltration for up to 28 days.

3.5 Osteogenic potential of scaffolds

Having established biocompatibility, the osteogenic potential of the composite scaffold was evaluated using the CI-nHA scaffold as a reference. The quantitative analysis of ALP expression shows no significant difference between the CI-nHA and composite groups (Figure 4a), where ALP activity significantly increased from 89.7 mg/DNA on day 7 to 593.4 mg/DNA on day 14 in the CI-nHA scaffold ($p < 0.0001$), and from 79.6 mg/DNA on day 7 to 465.3 mg/DNA on day 14 in the composite scaffold ($p < 0.001$). As a late-stage osteogenic marker, mineralization was further assessed by calcium deposition content (Figure 4b). Due to the presence of nHA, original calcium content was 239.6 μg/mL in cell-free CI-nHA scaffold and 261.9 μg/mL in cell-free composite scaffold. Notably, significantly enhanced mineralization by MC3T3 cells was observed, evidenced by the increased calcium content in both cell-seeded scaffolds on day 21 ($p < 0.01$) and day 28 ($p < 0.0001$), where highest calcium levels appeared on day 28, reaching 500.9 μg/mL in CI-nHA scaffold and 495.0 μg/mL in composite scaffold. Mineralization was further assessed using Alizarin Red S staining (Figure 4c). After 28 days of differentiation, dark red mineral deposits were evenly distributed in both the CI-nHA matrix and composite scaffold. Additionally, Figure 4d illustrates the relative expression of osteogenesis-related genes COL1A1, RUNX2, OCN, and BMP-2 after 21 days of differentiation. Gene expression levels in the composite scaffold were comparable to those in the CI-nHA scaffold, with no significant differences observed. These results demonstrate that the composite scaffold retains the osteogenic capacity of the CI-nHA matrix, effectively supporting ALP activity, mineralization, and bone-related gene expression.

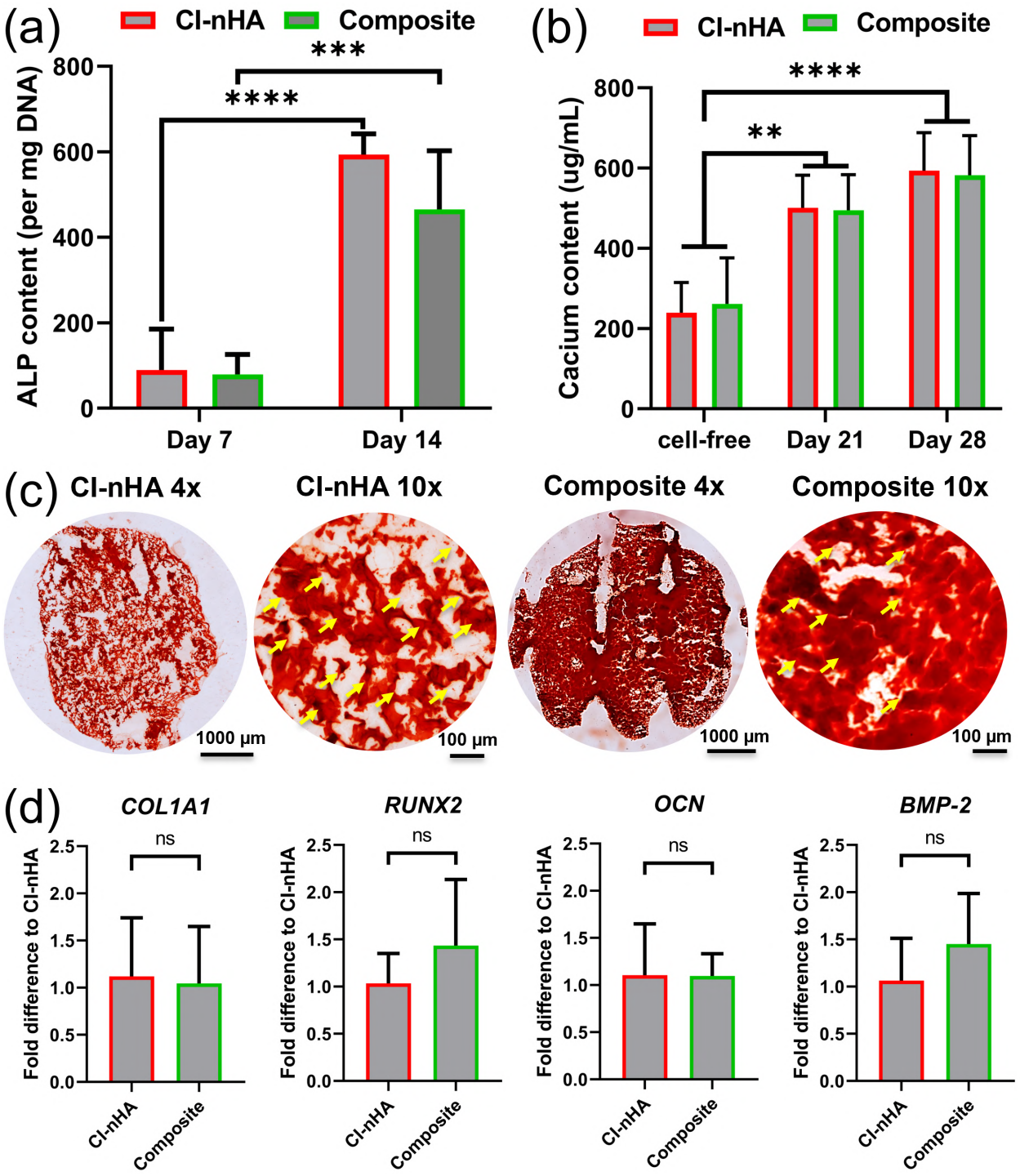

Figure 4. Osteogenic differentiation of MC3T3 cells on CI-nHA and composite scaffolds. (a) ALP content in MC3T3 cells cultured on scaffolds at day 7 and 14, (b) calcium content in MC3T3 cells on scaffolds at days 21 and 28, (c) Alizarin Red S histological staining at day 28, and (d) relative gene expression of COL1A1, RUNX2, OCN and BMP-2 at day 21.

3.6 Angiogenic potential of scaffolds

The angiogenic potential of the scaffolds was evaluated by culturing EA.hy 926 endothelial cells on CI-nHA and composite scaffolds for five days. Cell proliferation increased steadily from day 1 to day 5, with tube-like structures forming on both scaffolds, as shown in Figures 5 a-d. Moreover, after five days in culture, the expression levels of key vascular-related genes of VEGF, VE-cadherin, and MMP-2, remained comparable between the composite and CI-nHA scaffolds, with no significant differences (Figure 5e, f, and g), suggesting the presence of early angiogenic signals within this period. These findings confirm that the composite scaffold fully preserves the angiogenic properties of the CI-nHA matrix, supporting endothelial cell proliferation and vascularization.

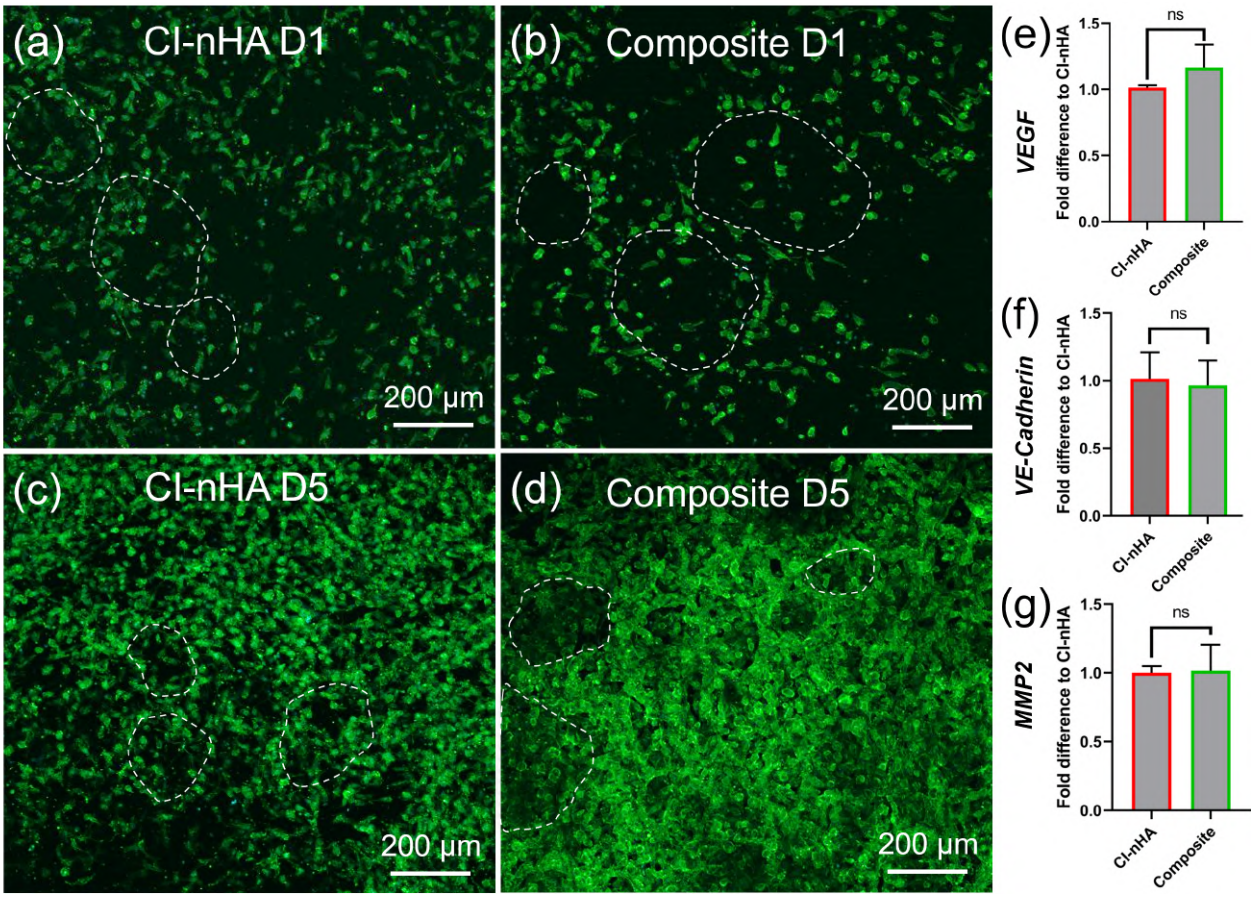

Figure 5. Angiogenic differentiation of EA.hy 926 cells on scaffolds. Confocal images of (a) cells on the CI-nHA scaffold at day 1, (b) cells on the composite scaffold at day 1, (c) cells on the CI-nHA scaffold at day 5, and (d) cells on the composite scaffolds at day 5; Relative gene expression of (e) VEGF, (f) VE-cadherin, and (g) MMP-2 of EA.hy 926 cells on both scaffolds after 5 days.

3.7 Cell viability and mineralization following *in vitro* mechanical stimulation

The effect of *in vitro* mechanical stimulation on the osteogenesis of MC3T3 cells cultured on the composite scaffold was studied using a bioreactor system with simulated conditions of native bone motive environment (Figure 6a). To assess the impact of mechanical stimulation on cell viability, the metabolic activity of cells seeded on scaffolds was monitored (Figure 6b). There is no compromised effect found after seven days of mechanical stimulation, compared to values before mechanical stimulation and after seeding. Moreover, qPCR analysis was further performed to check osteogenesis (Figure 6c). Compared to the mechanical stimulation group alone, both the chemical stimulation and double stimulation groups exhibited higher expression levels in all four genes, with a significant increase observed in COL1A1 ($p < 0.05$). While compared with the chemical stimulation group alone, the double stimulation group showed higher expression levels of ALP, OCN, and RUNX2. Notably, for OCN, a key marker of mineralization, a significantly high level was observed in double stimulation group than that of the chemical stimulation alone ($p < 0.01$). These results highlight the synergistic effect of both stimulations in enhancing osteogenesis at the early period of seven days.

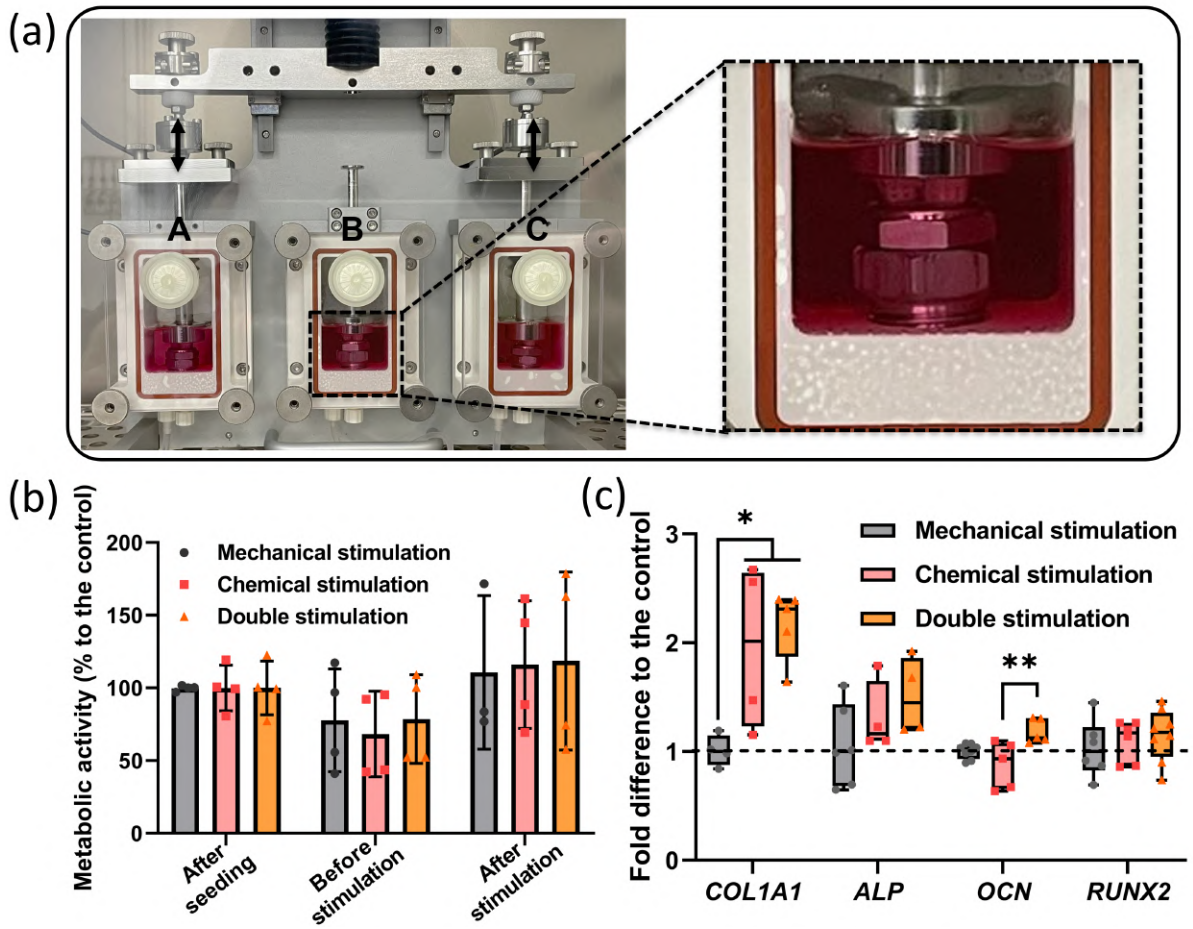

Figure 6. (a) Digital image of the bioreactor system used for cell culture with cyclic compression, (b) metabolic activity after seeding, before stimulation and after stimulation, and (c) relative gene expression of COL1A1, ALP, OCN, and RUNX2 of MC3T3 cell seeded on composite scaffolds after 7 days of mechanical stimulation.

4. Discussion

Traditional bone defect repair treatments are limited in their ability to treat large defects although the field of tissue engineering shows promise in providing alternative approaches for replacing damaged tissues. This study presents the development of a biomimetic composite scaffold by integrating a 3D-printed $PCE_{20k}C$ scaffold that provides mechanical reinforcement with a biomimetic and bioactive matrix (CI-nHA) composed of collagen type I and nano-hydroxyapatite to provide biological cues. The resulting composite scaffold meets the essential requirements for bone tissue engineering, including optimal morphology, mechanical strength, degradation properties, and enhanced osteogenesis and angiogenesis, making it a promising candidate for bone defect repair.

The composite scaffold was designed with biomimetic components and hierarchical porosity and successfully fabricated with excellent spatial integrity and uniform calcium distribution. The bioactive CI-nHA matrix consisting of collagen type I and nano-hydroxyapatite, closely mimics native bone composition, endowing the scaffold with outstanding osteoconductive properties [32]. Previous studies have confirmed that porous CI-nHA matrices support cells attachment and infiltration *in vitro* after 28 days [21] and facilitate osteogenesis and new bone formation in a rabbit model within 16 weeks [23]. In this work, the matrix was integrated into a 3D-printed $PCE_{20k}C$ scaffold featuring a well-connected and uniform pore structure. SEM and EDS images showed that the $PCE_{20k}C$ filaments were firmly surrounded by the porous CI-nHA matrix, with n-HA homogeneously distributed throughout. Porosity plays a critical role in bone regeneration. Studies have shown that pore sizes between 300 - 1000 μm facilitate cell infiltration, proliferation, migration, and nutrient and waste transport. Among them, larger pore sizes can enhance vascularization and direct bone formation but reduce cell seeding efficiency [18]. In this study, the 3D-printed $PCE_{20k}C$ scaffold with macropores of 963 μm was used as a framework, filled with porous collagen matrix with micropores of ~ 100 μm which facilitated cell adhesion. More importantly, the microstructure of the CI-nHA matrix remained unchanged after integration, compared with previous study [31], confirming that the $PCE_{20k}C$ framework did not alter its critical properties. Overall, the combination of biomimetic components and appropriate hierarchical porosity enhances its potential for bone defect repair.

Addressing mechanical requirements is a major challenge in the treatment of large bone defects. The composite scaffold overcomes this limitation with the integration of a stiff polymer structure to obtain desired mechanical properties. An ideal implant should have balanced mechanical properties, neither too weak to support damaged tissue nor excessively rigid, which could cause secondary fractures and impede tissue repair [11]. Bioactive collagen scaffolds demonstrate efficient bone repair potential but exhibit mechanical properties in the kPa range, which is insufficient to support new bone growth. Although some studies have attempted to enhance mechanical strength by mineralizing collagen or incorporating HA particles, most resulting scaffolds still fall short of native bone requirements [33]. In this study, the incorporation of the $PCE_{20k}C$ framework endowed the composite scaffold with a modulus of 37.0 MPa and a stress of 8 MPa, both of which fall within the range of cancellous bone (compressive modulus: 10 - 2000

MPa, compressive strength: 2 - 12 MPa) [34,35]. The modulus of the composite scaffold closely matched that of the $PCE_{20k}C$ framework (36.9 MPa), indicating that mechanical support was completely provided by the $PCE_{20k}C$ structure and was unaffected by the incorporation of the CI-nHA matrix. Compression tests in PBS solution further confirmed the mechanical stability of the scaffold in a wet environment, mimicking physiological conditions. These findings suggest that the composite scaffold possesses suitable and stable mechanical properties for bone repair applications.

Another critical factor that needs to be considered is the biomaterial degradation rate, which should well match the targeted tissue regeneration rate. Currently, 3D-printed bone scaffolds made from natural polymers, such as collagen, chitosan, and gelatin, degrade within a few weeks due to their high bioactivity, leading to a rapid loss of mechanical support and structural integrity. Conversely, synthetic polymer-based scaffolds, such as those made from PCL and PLA, degrade slowly over several months to years due to their high crystallinity, often remaining in the body long after bone regeneration is complete [9]. In this study, the composite scaffold exhibited an improved and controlled degradation process. The degradation mechanism of $PCE_{20k}C$ copolymer causes PEG_{20k} blocks within molecular chains to be initially dissolved and released, resulting in a rapid mass loss and the formation of a localized acidic environment. Subsequently, degradation was predominantly driven by PCL blocks, leading to a gradual slowdown in mass loss [36], as shown in Figure 2b and c. However, for the composite scaffold, the $PCE_{20k}C$ filaments were firmly wrapped by the CI-nHA matrix, which limited the release of dissolved $PEG_{20}k$, resulting in a slower mass loss than $PCE_{20k}C$ alone. Moreover, the release of nHA particles along matrix degradation also helped neutralize acidity, further stabilizing the degradation environment. Notably, although the release of $PCE_{20k}C$ was restricted, the hydrophilicity of the CI-nHA matrix accelerated internal $PEG_{20}k$ dissolution, forming voids within the $PCE_{20k}C$ filaments. This process ultimately led to scaffold fracture under 20% compression strain after eight weeks, as shown in Figure S3. Overall, CI-nHA matrix accelerated the degradation of the $PCE_{20k}C$ framework and improved the degradation microenvironment, allowing an appropriate degradation rate aligned with the native regeneration timeline of cancellous bone (6–8 weeks) [37], making it a promising candidate for bone regeneration.

Biologically, the composite scaffold maintains robust osteogenesis and angiogenesis comparable to the highly biologically functional unreinforced CI-nHA scaffold while offering improved mechanical and degradation properties. The integration of the $PCE_{20k}C$ framework had no adverse effects on osteoblast metabolic activity, viability and infiltration over 28 days of culture. Osteogenesis was confirmed through tests for early bone formation marker ALP, late matrix maturation marker calcium, and bone-related genes expression (COLI, RUNX2, OCN, and BMP-2), all of which showed consistent results with previous CI-nHA scaffold studies [38]. Notably, the 3D-printed $PCE_{20k}C$ framework helped to increase stiffness and expand internal space of CI-nHA matrix in composite scaffold, compared to CI-nHA scaffold alone, leading to the occurrence of mechanotransduction. This hypothesis was supported by higher expression of RUNX2 and BMP-2 genes observed in composite scaffold, which are activated by mechanotransduction through the YAP/TAZ and Wnt signaling pathways [39]. Additional evidence is the increased cell infiltration shown in H&E staining compared to CI-nHA scaffold. Bone tissue is highly vascularized. In the early stages of bone repair, vascularization plays a crucial role by supplying osteocytes with essential nutrients and supporting subsequent bone formation [40]. Previous studies have shown that CI-nHA-based scaffolds effectively stimulate MSC vascularization [38]. This study shows that the composite scaffold maintained comparable angiogenic capacity, as evidenced by tubular formation and the expression of vascular-related genes, including VEGF, VE-cadherin, and MMP-2. These findings suggest that the composite scaffold holds great potential to promote bone defect repair through osteogenic-angiogenic coupling.

Bone tissue is metabolically active and adapts to mechanical stress through remodeling, while mechanosensitive osteocytes sense and respond to mechanical stimulation, converting these signals into biochemical through molecular pathways that regulate osteogenic gene expression [41]. Therefore, understanding how *in vitro* mechanical stimulation affects osteogenesis of osteoblast-loaded composite scaffolds is beneficial for predicting their performance in an actual bone defect environment. To explore this, a dynamic compression bioreactor system was used to culture cell-loaded scaffolds under sterile compression conditions. The applied deformation was 0.1 mm, corresponding to a strain of 3.3%, which is within the elastic deformation range of the scaffold and promoting intramembranous bone formation range (below 5%) [42]. The compression frequency was set at 1 Hz, to simulate the normal walking motion of the human body. In our study,

after seven days of dynamic culture, early mineralization was observed in dynamic groups, compared to static culture. Previous study showed similar results of enhanced expression of Osteonectin and COL1A1 in MSC seeded on PCL-TCP scaffold after cyclic compression in the first week [29]. Another study also demonstrated that mechanical stimulation applied on type I collagen sponge scaffold promoted effective osteogenesis evidenced by increased calcium content and ash content after 14 days [43]. In addition, the effect of compression stimulation also on osteogenic differentiation was similar to those observed with osteogenic factor supplementation, indicating that mechanical stimulation alone also can effectively induce osteogenesis. This finding is also consistent with the results from Shin Kang et al. [44], who found that cyclic flexure deformation of 1 Hz applied to scaffold induced osteogenic differentiation without the addition of osteogenic triggers, as reflected by increased expression of osteopontin in human adipose-derived stem cells (ASCs). Based on the above osteogenesis results, we speculate that the possible molecular pathways that cause mechanical transduction in this study include integrin-mediated adhesion (FA), Wnt/β-catenin signaling pathway, π meson channel transduction, and TGF-β/BMP-2 pathway, as shown in Figure 7. Integrin-mediated adhesion plays a key role in sensing mechanical cues and transmitting them to intracellular signaling networks through focal adhesion kinase (FAK) activation, which subsequently regulates cytoskeletal remodeling and osteogenic gene expression [45]. In parallel, mechanical stimulation has been widely reported to activate canonical Wnt/β-catenin signaling, a central regulator of osteoblast differentiation and bone formation [46]. Recent studies also suggest that Piezo1/2 mechanosensitive ion channels play a critical role in load-induced Ca^{2+} influx and subsequent activation of osteogenic transcription programs [47]. Furthermore, the TGF-β/BMP-2 signaling closely associated with extracellular matrix remodeling and osteoblastic maturation, is known to be responsive to mechanical loading, thereby contributing to the regulation of osteogenesis under dynamic conditions [48]. However, the precise molecular mechanisms remain undetermined and require further investigation. Overall, the application of this bioreactor represents a significant step toward simulating the clinical microenvironment *in vitro*, providing valuable insights into biological performance of the scaffold.

Despite its promising findings, there are still some challenges. Dynamic perfusion of culture medium in the bioreactor should be considered, as it facilitates nutrient and waste exchange, thereby enhancing cell proliferation and promoting bone tissue repair. Moreover, future studies

should focus on optimizing bioreactor conditions by incorporating more sophisticated dynamic parameters. Furthermore, assessing the composite scaffold in animal models to evaluate its effectiveness in bone defect repair in the future is also important to provide critical data for translating this technology into clinical applications.

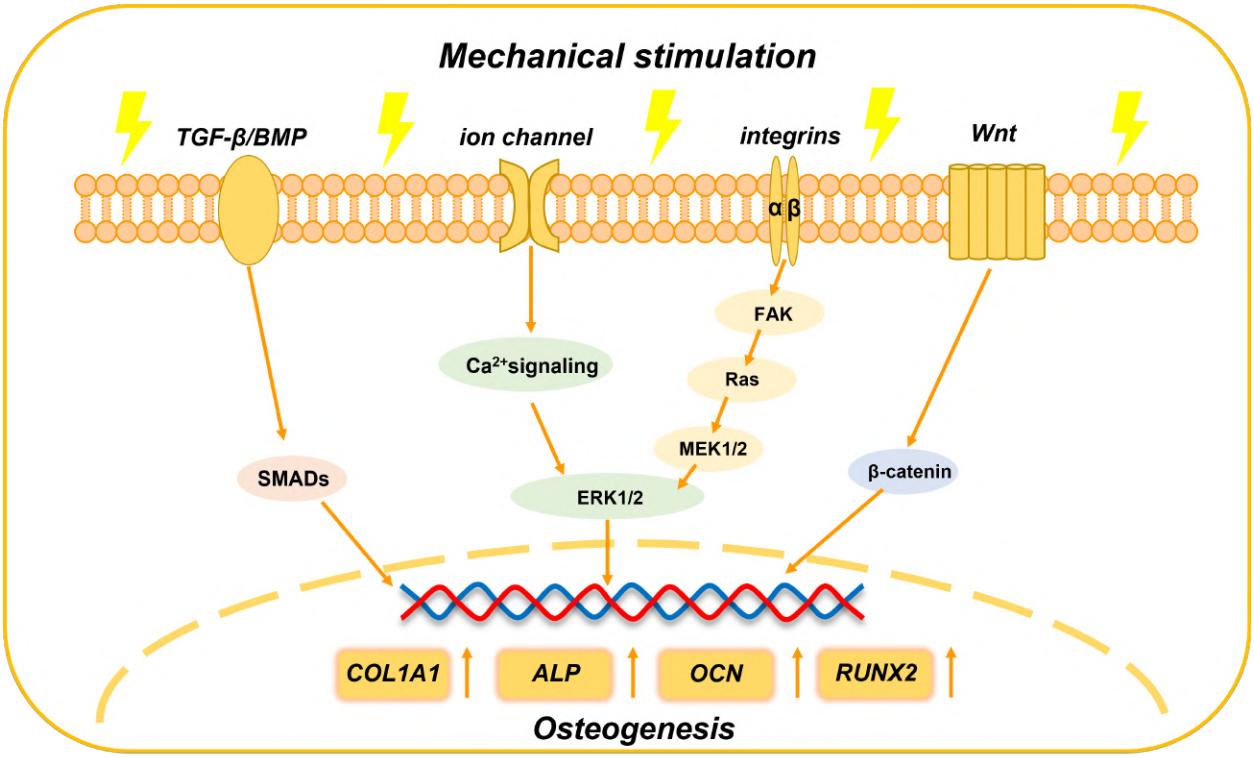

Figure 7. Potential molecular pathways of bone cells sensing and responding to mechanical stimulation

5. Conclusion

In summary, a novel reinforced scaffold was developed, in which the 3D printed $PCE_{20k}C$ framework served as mechanical reinforcement to allow application for bone repair and the CI-nHA matrix provided specific bioactivity for bone regeneration. The scaffold exhibited hierarchical architecture, mechanical properties similar to cancellous bone and a degradation rate matching the rate of new bone formation. The reinforced scaffold supported effective osteogenesis and angiogenesis, while supporting early mineralization under simulated physiological conditions, proving a new strategy for restoring large bone defects by combining precise 3D-printed structure with a bio-tailored matrix to meet the unique structural and biological requirements.

Acknowledgements

This study was supported by Spanish Research Agency through the grant PID2021-124389OB-C21 and European Research Council (ERC) Advanced Grant n°788753 (ReCaP, PI: FOB). Ms. Y. Liu acknowledges the support from the China Scholarship Council (CSC No. 202106990026). Dr. M. Echeverry-Rendón acknowledges the support of the Comunidad de Madrid through the "Talento César Nombela" project (2023-T1/TEC-29099). Scheme1 was partly created using templates provided by Servier Medical Art (https://smart.servier.com/), licensed under a Creative Commons Attribution 4.0 Unported License (https://creativecommons.org/licenses/by/4.0/).

Reference

[1] E.H. Schemitsch, Size Matters: Defining Critical in Bone Defect Size!, J. Orthop. Trauma. 31 (2017) S20–S22. https://doi.org/10.1097/BOT.0000000000000978.

[2] B. Chen, Z. Lin, Q. Saiding, Y. Huang, Y. Sun, X. Zhai, Z. Ning, H. Liang, W. Qiao, B. Yu, K.W.K. Yeung, J. Shen, Enhancement of critical-sized bone defect regeneration by magnesium oxide-reinforced 3D scaffold with improved osteogenic and angiogenic properties, J. Mater. Sci. Technol. 135 (2023) 186–198. https://doi.org/10.1016/j.jmst.2022.06.036.

[3] M. Mirkhalaf, Y. Men, R. Wang, Y. No, H. Zreiqat, Personalized 3D printed bone scaffolds: A review, Acta Biomater. 156 (2023) 110–124. https://doi.org/10.1016/j.actbio.2022.04.014.

[4] C. Wang, W. Huang, Y. Zhou, L. He, Z. He, Z. Chen, X. He, S. Tian, J. Liao, B. Lu, Y. Wei, M. Wang, 3D printing of bone tissue engineering scaffolds, Bioact. Mater. 5 (2020) 82–91. https://doi.org/10.1016/j.bioactmat.2020.01.004.

[5] G.L. Koons, M. Diba, A.G. Mikos, Materials design for bone-tissue engineering, Nat. Rev. Mater. 5 (2020) 584–603. https://doi.org/10.1038/s41578-020-0204-2.

[6] C. Xu, Z. Liu, X. Chen, Y. Gao, W. Wang, X. Zhuang, H. Zhang, X. Dong, Bone tissue engineering scaffold materials: Fundamentals, advances, and challenges, Chin. Chem. Lett. 35 (2024) 109197. https://doi.org/10.1016/j.cclet.2023.109197.

[7] B. Zhang, J. Li, L. He, H. Huang, J. Weng, Bio-surface coated titanium scaffolds with cancellous bone-like biomimetic structure for enhanced bone tissue regeneration, Acta Biomater. 114 (2020) 431–448. https://doi.org/10.1016/j.actbio.2020.07.024.

[8] D. Carluccio, A.G. Demir, M.J. Bermingham, M.S. Dargusch, Challenges and Opportunities in the Selective Laser Melting of Biodegradable Metals for Load-Bearing Bone Scaffold Applications, Metall. Mater. Trans. A Phys. Metall. Mater. Sci. 51 (2020) 3311–3334. https://doi.org/10.1007/s11661-020-05796-z.

[9] A. Kirillova, T.R. Yeazel, D. Asheghali, S.R. Petersen, S. Dort, K. Gall, M.L. Becker, Fabrication of Biomedical Scaffolds Using Biodegradable Polymers, Chem. Rev. 121 (2021) 11238–11304. https://doi.org/10.1021/acs.chemrev.0c01200.

[10] G. Turnbull, J. Clarke, F. Picard, P. Riches, L. Jia, F. Han, B. Li, W. Shu, 3D bioactive composite scaffolds for bone tissue engineering, Bioact. Mater. 3 (2018) 278–314. https://doi.org/10.1016/j.bioactmat.2017.10.001.

[11] L. Zhang, G. Yang, B.N. Johnson, X. Jia, Three-dimensional (3D) printed scaffold and material selection for bone repair, Acta Biomater. 84 (2019) 16–33. https://doi.org/10.1016/j.actbio.2018.11.039.

[12] G. BaoLin, P.X. Ma, Synthetic biodegradable functional polymers for tissue engineering: a brief review., Sci. China Chem. 57 (2014) 490–500. https://doi.org/10.1007/s11426-014-5086-y.

[13] Q. Dong, M. Zhang, X. Zhou, Y. Shao, J. Li, L. Wang, C. Chu, F. Xue, Q. Yao, J. Bai, 3D-printed Mg-incorporated PCL-based scaffolds: A promising approach for bone healing, Mater. Sci. Eng. C 129 (2021) 112372. https://doi.org/10.1016/j.msec.2021.112372.

[14] S. Wang, R. Gu, F. Wang, X. Zhao, F. Yang, Y. Xu, F. Yan, Y. Zhu, D. Xia, Y. Liu, 3D-Printed PCL/Zn scaffolds for bone regeneration with a dose-dependent effect on osteogenesis and osteoclastogenesis, Mater. Today Bio 13 (2022) 100202. https://doi.org/10.1016/j.mtbio.2021.100202.

[15] L.A. Bosworth, S. Downes, Physicochemical characterisation of degrading polycaprolactone scaffolds, Polym. Degrad. Stab. 95 (2010) 2269–2276. https://doi.org/10.1016/j.polymdegradstab.2010.09.007.
[16] Y.Y. Liu, J.P.F. Blazquez, G.Z. Yin, D.Y. Wang, J. Llorca, M. Echeverry-Rendón, A strategy to tailor the mechanical and degradation properties of PCL-PEG-PCL based copolymers for biomedical application, Eur. Polym. J. 198 (2023) 112388. https://doi.org/10.1016/j.eurpolymj.2023.112388.
[17] S. Wang, H. Chen, J. Huang, S. Shen, Z. Tang, X. Tan, D. Lei, G. Zhou, Gelatin-modified 3D printed PGS elastic hierarchical porous scaffold for cartilage regeneration, APL Bioeng. 7 (2023) 036105. https://doi.org/10.1063/5.0152151.
[18] R. Dong, M. Kang, Y. Qu, T. Hou, J. Zhao, X. Cheng, Incorporating Hydrogel (with Low Polymeric Content) into 3D-Printed PLGA Scaffolds for Local and Sustained Release of BMP2 in Repairing Large Segmental Bone Defects, Adv. Healthc. Mater. (2024) 2403613. https://doi.org/10.1002/adhm.202403613.
[19] P. Nitti, S. Kunjalukkal Padmanabhan, S. Cortazzi, E. Stanca, L. Siculella, A. Licciulli, C. Demitri, Enhancing Bioactivity of Hydroxyapatite Scaffolds Using Fibrous Type I Collagen, Front. Bioeng. Biotechnol. 9 (2021) 631177. https://doi.org/10.3389/fbioe.2021.631177.
[20] S. Rammelt, E. Schulze, M. Witt, E. Petsch, A. Biewener, W. Pompe, H. Zwipp, Collagen Type I Increases Bone Remodelling around Hydroxyapatite Implants in the Rat Tibia, Cells Tissues Organs 178 (2005) 146–157. https://doi.org/10.1159/000082245.
[21] G.M. Cunniffe, C.M. Curtin, E.M. Thompson, G.R. Dickson, F.J. O'Brien, Content-Dependent Osteogenic Response of Nanohydroxyapatite: An in Vitro and in Vivo Assessment within Collagen-Based Scaffolds, ACS Appl. Mater Interfaces. 8 (2016) 23477–23488. https://doi.org/10.1021/acsami.6b06596.
[22] F. David, T.J. Levingstone, W. Schneeweiss, M. de Swarte, H. Jahns, J.P. Gleeson, F.J. O'Brien, Enhanced bone healing using collagen–hydroxyapatite scaffold implantation in the treatment of a large multiloculated mandibular aneurysmal bone cyst in a thoroughbred filly, J. Tissue Eng. Regen. Med. 9 (2015) 1193–1199. https://doi.org/https://doi.org/10.1002/term.2006.
[23] F.G. Lyons, J.P. Gleeson, S. Partap, K. Coghlan, F.J. O'Brien, Novel Microhydroxyapatite Particles in a Collagen Scaffold: A Bioactive Bone Void Filler?, Clin. Orthop. Relat. Res. 472 (2014) 1318-1328. https://journals.lww.com/clinorthop/fulltext/2014/04000/novel_microhydroxyapatite_particles_in_a_collagen.41.aspx.
[24] Q. Ma, Z. Miri, H.J. Haugen, A. Moghanian, D. Loca, Significance of mechanical loading in bone fracture healing, bone regeneration, and vascularization, J. Tissue Eng. 14 (2023). https://doi.org/10.1177/20417314231172573.
[25] J. Wolff, Concept of the Law of Bone Remodelling, in: J. Wolff (Ed.), The Law of Bone Remodelling, Springer Berlin Heidelberg, Berlin, Heidelberg, 1986: p. 1. https://doi.org/10.1007/978-3-642-71031-5_1.
[26] Y. Sun, B. Wan, R. Wang, B. Zhang, P. Luo, D. Wang, J.J. Nie, D. Chen, X. Wu, Mechanical Stimulation on Mesenchymal Stem Cells and Surrounding Microenvironments in Bone Regeneration: Regulations and Applications, Front. Cell Dev. Biol. 10 (2022) 808303. https://doi.org/10.3389/fcell.2022.808303.

[27] M.L. Vainieri, D. Wahl, M. Alini, G.J.V.M. van Osch, S. Grad, Mechanically stimulated osteochondral organ culture for evaluation of biomaterials in cartilage repair studies, Acta Biomater. 81 (2018) 256–266. https://doi.org/10.1016/j.actbio.2018.09.058.
[28] H. Jasuja, S. Kar, D.R. Katti, K.S. Katti, Perfusion bioreactor enabled fluid-derived shear stress conditions for novel bone metastatic prostate cancer testbed, Biofabrication 13 (2021) 035004. https://doi.org/10.1088/1758-5090/abd9d6.
[29] A. Ravichandran, J. Lim, M.S.K. Chong, F. Wen, Y. Liu, Y.T. Pillay, J.K.Y. Chan, S.H. Teoh, In vitro cyclic compressive loads potentiate early osteogenic events in engineered bone tissue, J. Biomed. Mater. Res. B Appl. Biomater. 105 (2017) 2366–2375. https://doi.org/10.1002/jbm.b.33772.
[30] I.S.O., 2017 Implants for surgery-Homopolymers, copolymers and blends on poly(lactide)-In vitro degradation testing https://www.iso.org/standard/64565.html
[31] G.M. Cunniffe, G.R. Dickson, S. Partap, K.T. Stanton, F.J. O'Brien, Development and characterisation of a collagen nano-hydroxyapatite composite scaffold for bone tissue engineering., J. Mater. Sci. Mater. Med. 21 (2010) 2293–2298. https://doi.org/10.1007/s10856-009-3964-1.
[32] A. Tsuchiya, S. Sotome, Y. Asou, M. Kikuchi, Y. Koyama, T. Ogawa, J. Tanaka, K. Shinomiya, Effects of pore size and implant volume of porous hydroxyapatite/collagen (HAp/Col) on bone formation in a rabbit bone defect model, 55 (2008) 91-9. https://doi.org/10.11480/jmds.550111
[33] Y. Li, Y. Liu, R. Li, H. Bai, Z. Zhu, L. Zhu, C. Zhu, Z. Che, H. Liu, J. Wang, L. Huang, Collagen-based biomaterials for bone tissue engineering, Mater. Des. 210 (2021) 110049. https://doi.org/10.1016/j.matdes.2021.110049.
[34] Y. Yan, H. Chen, H. Zhang, C. Guo, K. Yang, K. Chen, R. Cheng, N. Qian, N. Sandler, Y.S. Zhang, H. Shen, J. Qi, W. Cui, L. Deng, Vascularized 3D printed scaffolds for promoting bone regeneration, Biomaterials 190–191 (2019) 97–110. https://doi.org/10.1016/j.biomaterials.2018.10.033.
[35] K.K. Gómez-Lizárraga, C. Flores-Morales, M.L. Del Prado-Audelo, M.A. Álvarez-Pérez, M.C. Piña-Barba, C. Escobedo, Polycaprolactone- and polycaprolactone/ceramic-based 3D-bioplotted porous scaffolds for bone regeneration: A comparative study, Mater. Sci. Eng. C 79 (2017) 326–335. https://doi.org/10.1016/j.msec.2017.05.003.
[36] M. Bartnikowski, T.R. Dargaville, S. Ivanovski, D.W. Hutmacher, Degradation mechanisms of polycaprolactone in the context of chemistry, geometry and environment, Prog. Polym. Sci. 96 (2019) 1–20. https://doi.org/10.1016/j.progpolymsci.2019.05.004.
[37] C. Cheng, D. Shoback, Mechanisms Underlying Normal Fracture Healing and Risk Factors for Delayed Healing, Curr. Osteoporos Rep. 17 (2019) 36–47. https://doi.org/10.1007/s11914-019-00501-5.
[38] J.M. Sadowska, M. Ziminska, C. Ferreira, A. Matheson, A. Balouch, J. Bogle, S. Wojda, J. Redmond, A. Elkashif, N. Dunne, H.O. McCarthy, S. Donahue, F.J. O'Brien, Development of miR-26a-activated scaffold to promote healing of critical-sized bone defects through angiogenic and osteogenic mechanisms, Biomaterials 303 (2023) 122398. https://doi.org/10.1016/j.biomaterials.2023.122398.
[39] Q. Zhou, S. Lyu, A.A. Bertrand, A.C. Hu, C.H. Chan, X. Ren, M.J. Dewey, A.S. Tiffany, B.A.C. Harley, J.C. Lee, Stiffness of Nanoparticulate Mineralized Collagen Scaffolds Triggers Osteogenesis via Mechanotransduction and Canonical Wnt Signaling, Macromol. Biosci. 21 (2021) 2000370. https://doi.org/10.1002/mabi.202000370.

[40] H. Liu, H. Chen, Q. Han, B. Sun, Y. Liu, A. Zhang, D. Fan, P. Xia, J. Wang, Recent advancement in vascularized tissue-engineered bone based on materials design and modification, Mater. Today Bio 23 (2023) 100858. https://doi.org/10.1016/j.mtbio.2023.100858.

[41] X. Huang, R. Das, A. Patel, T. Duc Nguyen, Physical Stimulations for Bone and Cartilage Regeneration, Regen. Eng. Transl. Med. 4 (2018) 216–237. https://doi.org/10.1007/s40883-018-0064-0.

[42] L.E. Claes, C.A. Heigele, Magnitudes of local stress and strain along bony surfaces predict the course and type of fracture healing, J. Biomech. 32 (1999) 255-266. https://doi.org/10.1016/S0021-9290(98)00153-5

[43] S.M. Tanaka, K. Tachibana, Frequency-Dependence of Mechanically Stimulated Osteoblastic Calcification in Tissue-Engineered Bone In Vitro, Ann. Biomed. Eng. 43 (2015) 2083–2089. https://doi.org/10.1007/s10439-014-1241-z.

[44] K. Shin Kang, Y. Hun Jeong, J. Min Hong, W.-J. Yong, J.-W. Rhie, D.-W. Cho, Flexure-Based Device for Cyclic Strain-Mediated Osteogenic Differentiation, J. Biomech. Eng. 135 (2013) 114501. https://doi.org/10.1115/1.4025103.

[45] M. Yang, L.-W. Xiao, E.-Y. Liao, Q.-J. Wang, B.-B. Wang, J.-X. Lei, The role of integrin-β/FAK in cyclic mechanical stimulation in MG-63 cells, Int. J. Clin. Exp. Pathol. 7 (2014) 7451-9. https://pubmed.ncbi.nlm.nih.gov/25550780.

[46] P. Duan, L.F. Bonewald, The role of the wnt/β-catenin signaling pathway in formation and maintenance of bone and teeth, Int. J. Biochem. Cell Biol. 77 (2016) 23–29. https://doi.org/10.1016/j.biocel.2016.05.015.

[47] J. Wang, Y.X. Sun, J. Li, The role of mechanosensor Piezo1 in bone homeostasis and mechanobiology, Dev. Biol. 493 (2023) 80–88. https://doi.org/10.1016/j.ydbio.2022.11.002.

[48] M. Wu, S. Wu, W. Chen, Y.P. Li, The roles and regulatory mechanisms of TGF-β and BMP signaling in bone and cartilage development, homeostasis and disease, Cell Res. 34 (2024) 101–123. https://doi.org/10.1038/s41422-023-00918-9.